Chemical Physics Letters 658 (2016) 287–292

Contents lists available at ScienceDirect

Chemical Physics Letters

journal homepage: www.elsevier.com/locate/cplett

Research paper

Matrix sublimation method for the formation of high-density amorphous ice

A. Kouchi [a,*], T. Hama [a], Y. Kimura [a], H. Hidaka [a], R. Escribano [b], N. Watanabe [a]

[a] Institute of Low Temperature Science, Hokkaido University, Sapporo 060-0819, Japan
[b] Instituto de Estructura de la Materia, Consejo Superior de Investigaciones Cientificas, IEM-CSIC, 28006 Madrid, Spain

ARTICLE INFO

Article history:
Received 18 May 2016
In final form 23 June 2016
Available online 24 June 2016

Keywords:
Matrix sublimation
Ice
High-density amorphous ice

ABSTRACT

A novel method for the formation of amorphous ice involving matrix sublimation has been developed. A CO-rich CO:H_2O mixed ice was deposited at 8–10 K under ultra-high vacuum condition, which was then allowed to warm. After the sublimation of matrix CO at 35 K, amorphous ice remained. The amorphous ice formed exhibits a highly porous microscale texture; however, it also rather exhibits a density similar to that of high-density amorphous ice formed under high pressure. Furthermore, unlike conventional vapor-deposited amorphous ice, the amorphous ice is stable up to 140 K, where it transforms directly to cubic ice Ic.

1. Introduction

The importance of amorphous ice is widely recognized in the fields of physics, chemistry [1,2], and cryobiology [3], but is of particular interest in planetary science and astrophysics [4]. Various procedures for the preparation of amorphous ice have been developed in order to investigate the relationship between its structure and method of formation [2] (Fig. 1). Vapor deposition methods were often applied to prepare amorphous solid water (ASW) in a vacuum [5,6]. When water (H_2O) vapor is deposited onto a surface below 40 K, high-density ASW can be produced. In contrast, deposition at 40–70 K results in low-density ASW [6,7]. Unique property of ASW that is distinct from other amorphous ices is that ASW has larger surface area and higher porosity [8,9]. Rapid cooling of micron-sized water droplets or thin film can form amorphous ice referred to as hyperquenched glassy water (HGW) [10,11]. HGWs formed at ambient and high pressures are low- and high-density forms, respectively [12].

Disruption of ice crystals by compression or irradiation with high-energy particles is also known as formation method of amorphous ice [13–16]. High-density amorphous ice (HDA), which is distinct from the ASW and HGW formed at low pressures, could be formed by compression of ice crystals at high pressure [13,14]. HDA transforms low-density amorphous ice (LDA) by warming up at ambient pressure. Ice crystal in a vacuum can be amorphized by the irradiation with high-energy electron beam [15] or UV-rays at low temperature [16].

Since the structure of amorphous ice has been found to strongly depend on the method of its formation [2,17–19] and formation conditions [2,6,7,12], as described above, unknown amorphous ice structures may still be discovered through new formation methods. In this Letter, we report a new method for the formation of amorphous ice, matrix sublimation method. Remarkably, ice prepared by sublimation of a carbon monoxide (CO) matrix from a H_2O/CO mixture at around 35 K shows a highly porous texture different from that of ASW, and a density similar to that of HDA prepared under high pressure. This new method contributes to our understanding of the structure and physical properties of amorphous ice and to the development of new materials.

2. Experimental

Amorphous ice was prepared according to a newly developed matrix sublimation method, illustrated in Fig. 2. We observed this process *in situ* using the ultra-high vacuum (UHV) transmission electron microscope (TEM) and Fourier-transform infrared (FTIR) spectrometry.

A specially designed UHV TEM (JEOL JEM-2100V) for *in situ* observation of ice was developed following Kondo et al. [20]. Since the specimen was surrounded by a liquid nitrogen shroud, the pressure around the specimen was lower than the pressure of the specimen chamber (1×10^{-6} Pa). We used a liquid He cooling holder (Gatan ULTST) for specimen cooling, and a 5-nm-thick amorphous Si film (SiMPore Inc.) as a substrate for sample

* Corresponding author.
E-mail address: kouchi@lowtem.hokudai.ac.jp (A. Kouchi).

http://dx.doi.org/10.1016/j.cplett.2016.06.066
0009-2614/

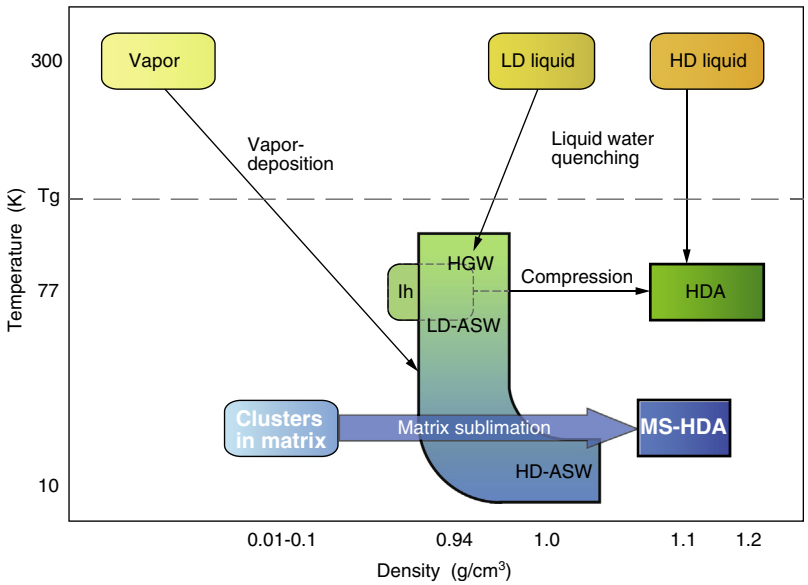

Fig. 1. Temperature-density diagram schematic of the formation of amorphous ices. The starting materials are shown in rounded rectangles, formation routes as arrows with names of methods, and products in rectangles. T_g is the glass transition temperature. HD-ASW, high-density amorphous solid water; LD-ASW, low-density amorphous solid water; HGW, hyperquenched glassy water; HDA, high-density amorphous ice; HD, high density; LD, low density; MS-HDA, matrix-sublimated high-density amorphous ice; Ih, hexagonal ice.

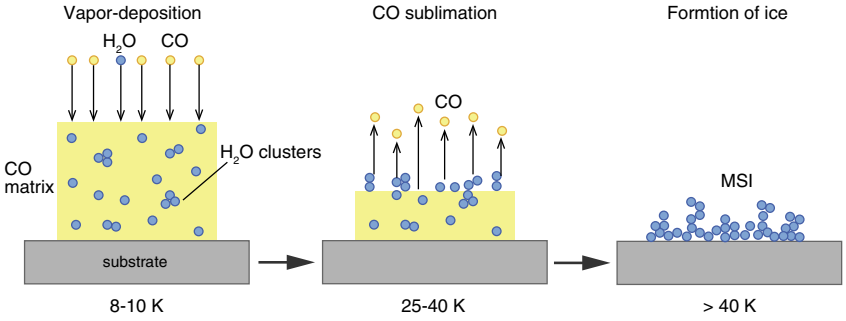

Fig. 2. Matrix sublimation method. Deposition of CO:H_2O on an 8–10 K substrate in an ultra-high vacuum chamber. After deposition, the substrate is warmed at a constant rate. Sublimation of matrix CO at 25–40 K. Formation of MSI at $T > 40$ K.

deposition. Of the three ports directed at the specimen surface, the one with an incident angle of 55° was used for a Ti gas inlet tube (inner diameter = 0.4 mm).

CO was used as the matrix because it is an astrophysically important molecule, active for IR spectroscopy, and could be evacuated by ion pumps equipped with a TEM. Mixtures of CO and H_2O at ratios of 50:1 and 10:1 were deposited on the Si thin film at about 8 K. We did not record TEM images during deposition to avoid damage from the electron beam. After deposition, the sample substrate was warmed at a rate of approximately 2.0 K/min, controlled manually. TEM images could not be recorded during the sublimation of CO because the pressure was higher than 10^{-4} Pa. The thickness of the ice samples remaining after CO sublimation was several tens of nanometres. To avoid electron-beam damage to the sample, a low-dose imaging technique was applied in which the accelerating voltage was 80 kV, the electron beam current was less than 0.1 pA/cm^2 and low magnification images were recorded using a CCD camera (Gatan ES500W). Furthermore, subsequent observations were taken from different positions of the sample. The edge of a single crystalline Si grid was used for the calibration of length in the analysis of the electron diffraction patterns.

For FTIR spectroscopy, we used a laboratory setup for surface reactions in interstellar environments (LASSIE) apparatus, as described previously [21]. The samples were prepared using a background deposition method on an Al substrate cooled to 10 K by He refrigeration. After deposition, the sample substrate was warmed at a rate of 2.0 K/min. IR spectra of samples were obtained and monitored by reflection–absorption spectroscopy. Typical column density of the samples after CO sublimation was 1.5×10^{16} molecules/cm^2.

3. Results and discussion

As shown in Fig. 3a, the CO:H_2O ice deposited at 8 K is a mixture of crystalline α-CO and a small amount of amorphous CO. Water molecules are embedded in the CO matrix as clusters (see Supplementary Fig. 1 and Supplementary Table 1. [22–24]). After the sublimation of CO at 25–40 K, we observed highly porous ice, as shown in Figs. 3b and 4; we term this the matrix-sublimated ice (MSI). The MSI shows wide textural variety at the micro- and submicroscale, with the ice exhibiting mainly concrete-like (Fig. 4a) or granite-like (Fig. 4c) textures, along with some minor occurrences of feather-like (Fig. 4b) or seaweed-like (Fig. 4d) textures. Conversely, these types of structures (micro- and submicroscale highly porous structures) are not observed in pure H_2O vapor-deposited

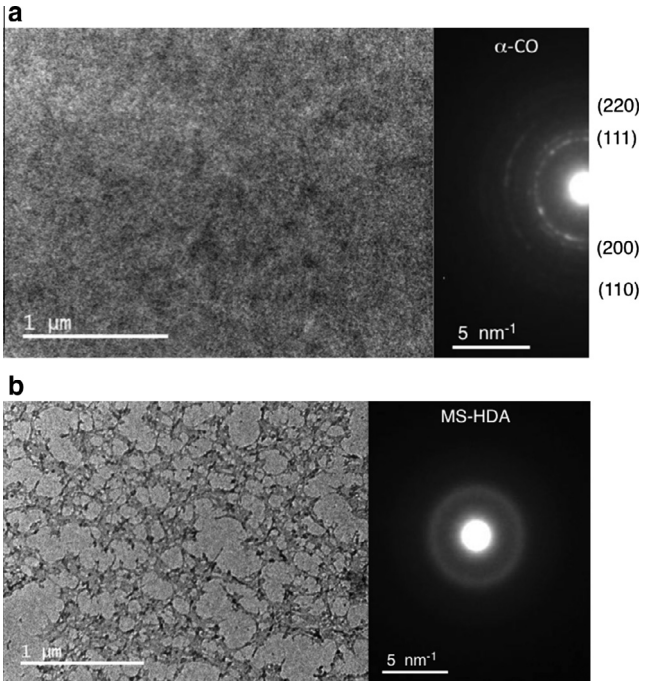

Fig. 3. Low-magnification TEM image and corresponding electron diffraction pattern of initial CO:H_2O = 10:1 ice at 8 K (a), and MS-HDA at 80 K (b). Electron diffraction pattern was obtained from the central circle region of 0.6 μm diameter.

amorphous ice, that is, ASW, as shown in Fig. 5. In addition, no temperature dependence on the structure of ASW was observed until crystallization occurs. However, the previous studies reported that ASW has larger surface area and higher porosity at lower temperatures, and it becomes less porous as the temperature increases [8,9]. We speculate that the space scales of porous structures are different between ASW (nanometer scale) and MS-HDA (micrometer scale), and the magnification in the present observation by TEM is too low to explicitly observe the porous structures of ASW. These results confirm that the formation of the highly porous MSI observed in the present study is not due to electron beam irradiation during TEM but due to intrinsic phenomena. This is further confirmed by IR measurements, in which a destructive beam is not applied, as discussed later.

As described below, we have confirmed that the structure of our MSI is that of an HDA ice, and have therefore termed it matrix-sublimated high-density amorphous (MS-HDA) ice. Fig. 6 shows the temperature dependence of the d-spacing in the main halo for vapor-deposited ASW and MS-HDA ice. In ASW, the d-spaces of the main peak increase with temperature, as observed by Jenniskens and Blake [6]. They assigned the lower and higher temperature forms as high-density ASW (HD-ASW) and low-density ASW (LD-ASW), respectively. Conversely, the d-spacing in the MS-HDA ice does not change with temperature, and remains constant at ca. 0.31 nm irrespective of whether the initial ice composition (CO:H_2O) is 10:1 or 50:1. Winkel et al. reported that the d-spaces in HDA ice made by submitting ice Ih to high pressure ranged from 0.28 to 0.32 nm [18], and the d-spaces of 0.31 nm for MS-HDA ice fall within this range. The density of MS-HDA ice is estimated to be 1.16 g/cm^3 from the relationships of d-spaces with pressure (0.1 GPa) [18], and pressure with density [25,26]. Mishima et al. have reported that the density of HDA ice at ambient pressure is 1.17 g/cm^3 [13]. Thus, we conclude that the MS-HDA ice generated in the present study is a high-density form similar to HDA ice produced under high pressure, but different from HD-ASW produced by vapor-deposition in a vacuum.

MS-HDA ice formed at around 35 K is very stable against temperature change up to 140 K. At temperatures around 140 K, MS-HDA ice directly transforms into ice Ic (Fig. 7). The transformation of HDA ice during heating depends on the initial formation conditions, annealing conditions, pressure and heating rate. Consequently, different transformation sequences (e.g. HDA → LDA → ice Ic and HDA → ice Ic) have been observed [27–29]. Although direct comparison between MS-HDA ice and HDA ice is difficult, it is worth noting that the behavior of MS-HDA ice observed in

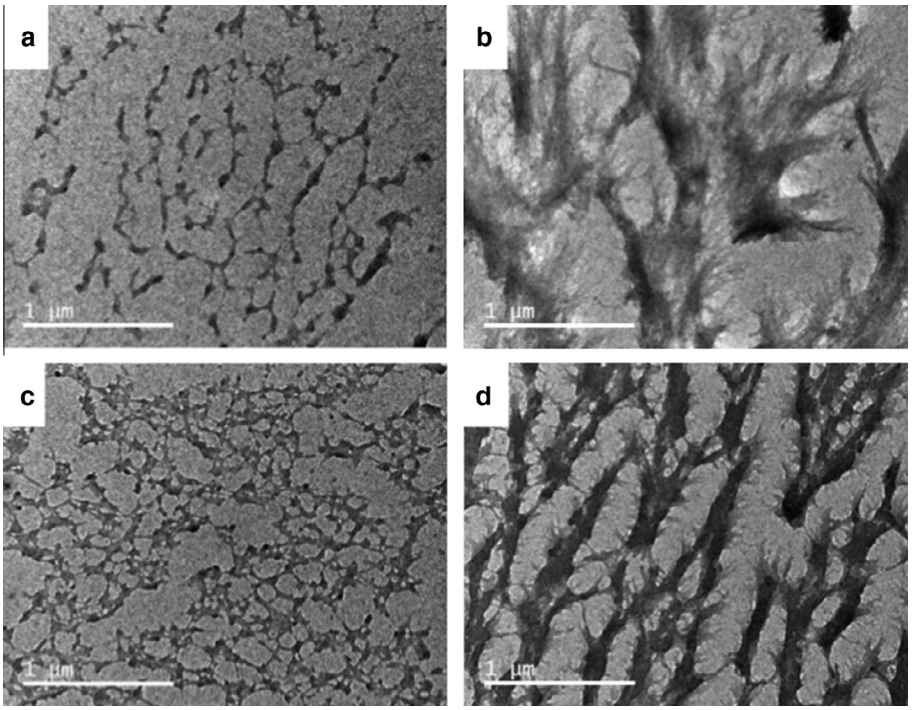

Fig. 4. Textural variety in highly porous MS-HDA ice. Generally, the black part is thicker and white part thinner. (a and b) Initial CO:H_2O = 50:1. (c and d) Initial CO:H_2O = 10:1. (Formation temperatures: a, 43 K; b, 36 K; c, 87 K; and d, 34 K.)

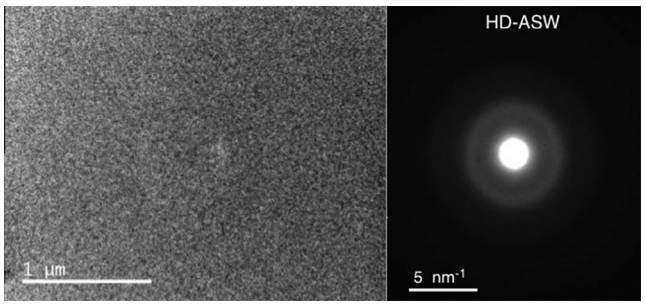

Fig. 5. Low-magnification TEM image and corresponding electron diffraction pattern of vapor-deposited ASW at 10 K.

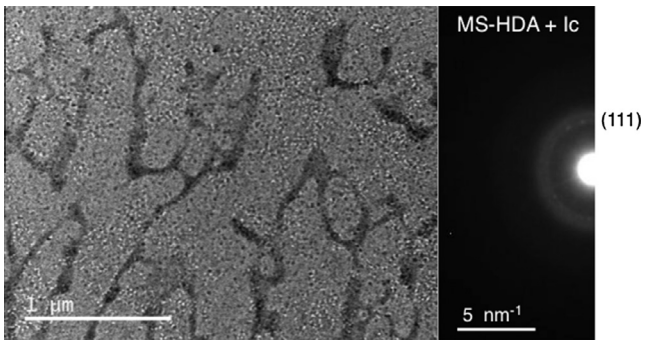

Fig. 7. Transformation from MS-HDA to ice Ic. Low-magnification TEM image and corresponding electron diffraction pattern of MS-HDA ice and ice Ic at 136 K.

the present study resembles that of HDA ice formed at 0.1 GPa [27] rather than that formed at 0.001 GPa.

Fig. 8 and Supplementary Fig. 1 show the changes in the FTIR spectra with temperature for ice of three different initial CO:H_2O ratios, i.e. 50:1, 10:1 and pure H_2O (ASW). A summary of the assignments is given in Supplementary Table 1. At low temperatures (10 and 20 K), monomers are present in the 50:1 ice, as the ν_3 asymmetric and ν_1 symmetric stretching modes of H_2O monomers are observed at 3707 cm^{-1} and 3617 cm^{-1}, respectively. However, no monomers are indicated in the 10:1 ice, but strong absorptions due to polymeric aggregates are observed (Supplementary Table 1). During the sublimation of CO around 30 K, the intensity of the water cluster bands decreases suddenly, and the characteristic OH stretching band at 3000–3600 cm^{-1} of solid water ice becomes stronger. After the sublimation of CO, MS-HDA ice remains. The spectral characteristics of the OH stretching band clearly differ between MS-HDA ice and ASW (Fig. 8). The spectral features and peak wavenumbers of MS-HDA ice made from the CO:H_2O mixture at ratios of 50:1 (Fig. 8a and b) and 10:1 (Fig. 8c and d) do not change with temperature, indicating the stability of MS-HDA ice. Conversely, those of vapor-deposited ASW changes as the temperature increases (Fig. 8e and f) [22], indicating that HD-ASW deposited at 10 K is relatively unstable. Dangling-OH bonds were observed in the IR spectra of MS-HDA ice and vapor-deposited ASW (Supplementary Fig. 2) [30]. These spectroscopic results imply that MS-HDA has porous structures like ASW at nanometer scale, in addition to the porous structures at micrometer scale as shown in Fig. 5.

Although we cannot precisely clarify the formation mechanism of MS-HDA ice, the following rationales are presented: The Laplace pressure of a 1.0 nm radius fine particle of MS-HDA ice is 0.14 GPa if we assume that its surface tension 70 mN/m. This pressure is similar to the lowest pressures at which HDA ice is formed. Thus, water aggregates of a few nanometres in diameter may be formed with high internal density. Another possibility is that the stress in the crystalline α-CO matrix plays an important role, as is acknowledged for thin films [31]. The stress in the solid could force the water molecules to be segregated into high-density pores.

The matrix sublimation method developed in the present study is a novel means of forming amorphous ice and supplements previously known methods. In vapor deposition and liquid water quenching, the surface temperature of the amorphous ice becomes higher owing to the heat of condensation [32] and solidification, respectively, which can sometimes lead to the crystallization. Conversely, in the matrix sublimation method, the sample surface is cooled owing to the sublimation heat of the matrix. In the high-pressure compression of ice crystals, transformation to amorphous ice is limited at temperatures higher than 77 K, and in irradiation methods, decomposition of water molecules is unavoidable.

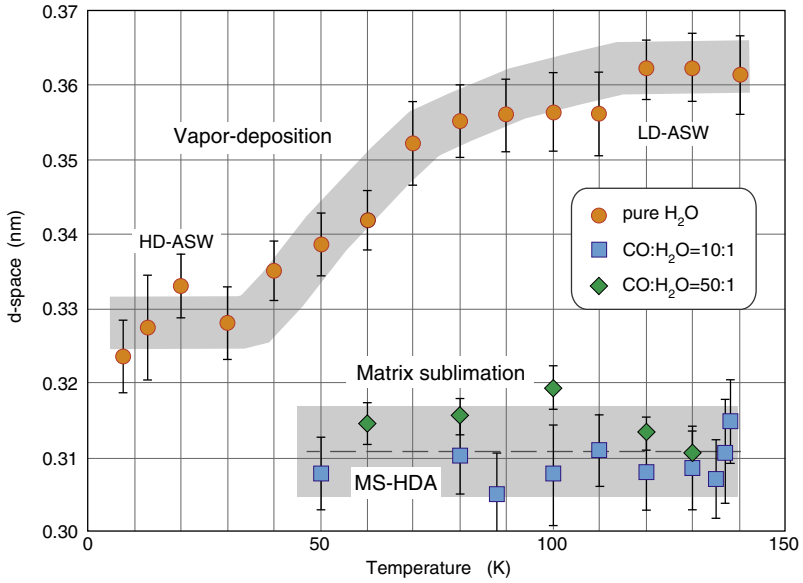

Fig. 6. Temperature dependence of d-spacing in the main halo of the electron diffraction patterns of amorphous ices. ASW (orange circles) and MS-HDA ice (blue squares: CO:H_2O = 10:1, green diamonds: CO:H_2O = 50:1).

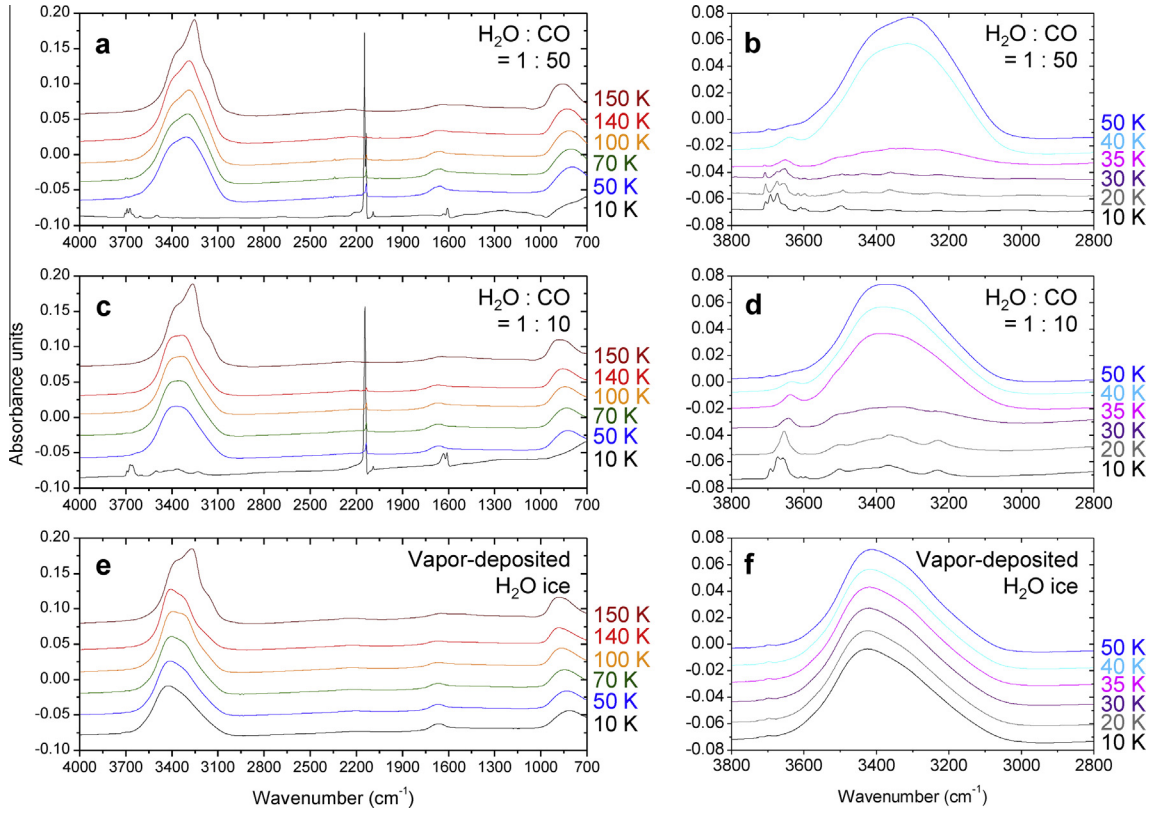

Fig. 8. Reflection–absorption IR spectra at different temperatures. (a and b) Initial composition of CO:H_2O = 50:1. (c and d) Initial composition of CO:H_2O = 10:1. (e and f) Pure H_2O. (b, d, and f) The change in the OH stretching bands between 10 and 50 K.

However, in the matrix sublimation method, no decomposition of water molecules occurs, and there is no temperature limit if we choose a suitable matrix species.

It may be possible to easily make other amorphous and crystalline ices that usually require a wide pressure range using modifications of the present matrix sublimation method with, for example, various ratios of matrix to water, various types of matrix (i.e. those formed at different sublimation temperatures or with different polarity materials), and various matrix sublimation rates. To explore the effect of the matrix to water ratio, we performed experiments using ices formed at CO:H_2O ratios of 10:1, 50:1 and 2:1, and ASW. A comparison of the d-spacing in the MSIs prepared using these ratios is presented in Supplementary Fig. 3. It is clear that the size of the d-spaces in the MSI prepared using a CO:H_2O ratio of 2:1 lies between those of MS-HDA ice and ASW, suggesting that the MSI prepared using the 2:1 ratio is a mixture of MS-HDA ice and ASW. We also performed experiments using N_2 for the matrix instead of CO, and similar results are obtained, although the d-spaces are slightly larger (Supplementary Fig. 4). These results clearly indicate that the interaction between the water and matrix molecules plays an essential role in determining the structure of the ice formed.

The most prominent feature of the matrix sublimation method is that high-pressure phases are formed very easily in a vacuum, whereas highly energetic processes such as ionization or high-temperature heating are required for other low-pressure syntheses, such as those of diamond or cubic boron nitride. Furthermore, this method may be applied to prepare other crystalline and amorphous solids. In fact, any laboratory that currently performs matrix isolation spectroscopy could also perform matrix sublimation preparation, as the apparatus needed for these techniques is essentially the same. Consequently, rapid progress in research into the formation of new materials is now possible.

4. Astrophysical implications

This study also has astrophysical implications, as CO-rich ices have been observed in icy grains within interstellar molecular clouds [33]. These grains consist of a silicate core, an inner mantle of organic refractory material, H_2O-rich amorphous ice, and a CO-rich outer mantle [34]. When CO sublimes due to the slight temperature increase during the formation of protoplanetary disks, highly porous MS-HDA ice is formed. The high porosity of icy grains could have a significant effect on the aggregation of interstellar grains and the physical properties of planetesimals. Therefore, the thermal conductivity of cometary nuclei might be smaller than has been thitherto thought [32]. Furthermore, the high porosity characteristics of cometary nuclei as observed by the Rosetta mission [35] could be explained by the aggregation of highly porous MS-HDA-covered icy grains. CO or N_2-rich ices are also observed on the surface of dwarf planets and icy satellites [36,37]. If CO or N_2 sublimes from these ices upon slight temperature increase, highly porous MS-HDA ice might be formed on the surface of these bodies.

Acknowledgments

We thank O. Mishima for critical reading of the manuscript, and S. Nakatsubo, K. Fujita, K. Sinbori and M. Ikeda for their help in the development of UHV-TEM. This study was supported by the Grant for the Joint Research Program of the Institute of Low Temperature

Science, Hokkaido University, I-link-1027 project from CSIC, JSPS KAKENHI (Grant Number 25247086), and MEXT KAKENHI (Grant Number 25108002).

Appendix A. Supplementary material

Supplementary data associated with this article can be found, in the online version, at http://dx.doi.org/10.1016/j.cplett.2016.06.066.

References

[1] V.F. Petrenko, R.W. Whitworth, Physics of Ice, Oxford Univ. Press, 1999.
[2] C.A. Angell, Ann. Rev. Phys. Chem. 55 (2004) 559.
[3] A. Cavalier, D. Spehner, B.M. Humbel (Eds.), Handbook of Cryo-Preparation Methods for Electron Microscopy, CRC Press, 2009.
[4] R.M.E. Mastrapa, W.M. Rundy, M.S. Gudipati, in: M.S. Gudipati, J. Castillo-Rogez (Eds.), The Science of Solar System Ices, Springer, 2013, p. 371.
[5] E.F. Burton, W.F. Oliver, Proc. R. Soc. Lond. A153 (1935) 166.
[6] P. Jenniskens, D.F. Blake, Science 265 (1994) 753.
[7] A.H. Narten, C.G. Vekatesh, J.A. Rice, J. Chem. Phys. 64 (1976) 1106.
[8] E. Mayer, R. Pletzer, Nature 319 (1986) 298.
[9] K.P. Stevenson, G.A. Kimmel, Z. Dohnalek, R.S. Smith, B.D. Kay, Science 283 (1999) 1505.
[10] P. Brüggeller, E. Mayer, Nature 288 (1980) 569.
[11] J. Dubochet, A.W. McDowell, J. Microsc. 124 (1981) RP3.
[12] O. Mishima, Y. Suzuki, J. Chem. Phys. 115 (2001) 4199.
[13] O. Mishima, L.D. Calvert, E. Whalley, Nature 310 (1984) 393.
[14] T. Loerting, C.G. Salzmann, I. Kohl, E. Mayer, A. Hallbrucker, Phys. Chem. Chem. Phys. 3 (2001) 5355.
[15] J. Lepault, R. Freeman, J. Dubochet, J. Microsc. 132 (1983) RP3.
[16] A. Kouchi, T. Kuroda, Nature 344 (1990) 134.
[17] O. Mishima, H.E. Stanley, Nature 396 (1998) 329.
[18] K. Winkel, M.S. Elsaesser, E. Mayer, T. Loerting, J. Chem. Phys. 128 (2008) 044510.
[19] C.A. Angel, Science 319 (2008) 582.
[20] Y. Kondo, K. Ohi, Y. Ishibashi, H. Hirano, Y. Harada, K. Takayanagi, Ultramicroscopy 35 (1991) 111.
[21] N. Watanabe, T. Shiraki, A. Kouchi, Astrophys. J. Lett. 588 (2003) L121.
[22] W. Hagen, A.G.G.M. Tielens, J.M. Greenberg, Chem. Phys. 56 (1981) 367.
[23] A. Givan, A. Loewenschuss, C.J. Nielsen, J. Chem. Soc. Faraday Trans. 92 (1996) 4927.
[24] A. Givan, A. Loewenschuss, C.J. Nielsen, Vib. Spectrosc. 16 (1998) 85.
[25] C.G. Salzmann, T. Loerting, S. Klotz, P.W. Mirwald, A. Hallbrucker, E. Mayer, Phys. Chem. Chem. Phys. 8 (2006) 386.
[26] T. Loerting, C.G. Salzmann, K. Winkel, E. Mayer, Phys. Chem. Chem. Phys. 8 (2006) 2810.
[27] O. Mishima, J. Chem. Phys. 100 (1994) 5910.
[28] P.H. Handle, M. Seidl, T. Loeting, Phys. Rev. Lett. 108 (2012) 225901.
[29] M. Seidl, K. Amann-Winkel, P.H. Handle, G. Zifferer, T. Loerting, Phys. Rev. B 88 (2013) 174105.
[30] V. Buch, J.P. Devlin, J. Chem. Phys. 94 (1991) 4091.
[31] F. Spaepen, Acta Mater. 48 (2000) 31.
[32] A. Kouchi, J.M. Greenberg, T. Yamamoto, T. Mukai, Astrophys. J. Lett. 388 (1992) L73.
[33] W.F. Thi, K.M. Pontoppidan, E.F. van Dishoeck, E. Dartois, L. d'Hendecourt, Astron. Astrophys. 394 (2002) L27.
[34] M. Spaans, P. Ehrenfreund, in: P. Ehrenfreund, K. Krafft, H. Kochan, V. Pirronello (Eds.), Laboratory Astrophysics and Space Research, Kluwer Academic Publisher, 1999, p. 1.
[35] W. Kofman et al., Science 349 (2015). aab0639-1.
[36] T.C. Owen, T.L. Roush, D.P. Cruikshank, J.L. Elliot, L.A. Young, C. de Bergh, B. Schmitt, T.R. Geballe, R.H. Brown, M.J. Bartholomew, Science 261 (1993) 745.
[37] W.M. Grundy, L.A. Young, J.A. Stansberry, M.W. Buie, C.B. Olkin, E.F. Young, Icarus 205 (2010) 594.